# Striatal dopamine synthesis capacity and neuromelanin in the substantia nigra: a multimodal imaging study in schizophrenia and healthy controls

Hooijdonk, C.F.M. van; Pluijm, M. van der; Smith, C.; Yaqub, M.; Velden, F.H.P. van; Horga, G.; ... ; Giessen, E. van de

Neuroscience Applied 2 (2023) 101134

Contents lists available at ScienceDirect

Neuroscience Applied

journal homepage: www.journals.elsevier.com/neuroscience-applied

Research Articles

# Striatal dopamine synthesis capacity and neuromelanin in the substantia nigra: A multimodal imaging study in schizophrenia and healthy controls

Carmen F.M. van Hooijdonk [a,b,*], Marieke van der Pluijm [c,g], Charlotte Smith [d], Maqsood Yaqub [d], Floris H.P. van Velden [e], Guillermo Horga [f], Kenneth Wengler [f], Monja Hoven [g], Ruth J. van Holst [g], Lieuwe de Haan [g], Jean-Paul Selten [a,b], Therese A.M.J. van Amelsvoort [a], Jan Booij [c], Elsmarieke van de Giessen [c,h]

[a] Department of Psychiatry and Neuropsychology, School for Mental Health and Neuroscience (MHeNs), University of Maastricht, Maastricht, the Netherlands
[b] Rivierduinen, Institute for Mental Health Care, Leiden, the Netherlands
[c] Department of Radiology and Nuclear Medicine, Amsterdam UMC, University of Amsterdam, Amsterdam, the Netherlands
[d] Department of Radiology and Nuclear Medicine, Amsterdam UMC, location Vrije Universiteit Medical Center, Amsterdam, the Netherlands
[e] Department of Radiology, Leiden University Medical Center, Leiden, the Netherlands
[f] Department of Psychiatry, New York State Psychiatric Institute, Columbia University, New York, NY, USA
[g] Department of Psychiatry, Amsterdam UMC, University of Amsterdam, Amsterdam, the Netherlands
[h] Amsterdam Neuroscience, Brain Imaging, Amsterdam, the Netherlands

ARTICLE INFO

Handling Editor: Prof. A. Meyer-Lindenberg

*Keywords:*
Neuromelanin
Substantia nigra
Dopamine synthesis capacity
Striatum
Schizophrenia

ABSTRACT

[$^{18}$F]F-DOPA PET is an established *in-vivo* method for investigating striatal dopamine synthesis capacity (DSC) and has demonstrated abnormalities in striatal DSC in schizophrenia. Neuromelanin-sensitive MRI (NM-MRI) is a promising, more accessible, tool that indirectly assesses dopaminergic functioning in the substantia nigra (SN). However, how [$^{18}$F]F-DOPA PET and NM-MRI, as measures of nigrostriatal dopaminergic functioning, interrelate is still unknown. We hypothesize that NM-MRI signal in the SN is positively correlated with striatal DSC in patients with a schizophrenia spectrum disorder (SSD) and healthy controls (HC). We acquired NM-MRI and dynamic [$^{18}$F]F-DOPA PET scans in 12 patients with SSD and 16 HC. In both groups, we assessed the correlation between nigral NM-MRI signal and DSC in the whole, associative, limbic, and sensorimotor striatum using voxelwise analyses within the SN. In HC, we found subsets of voxels within the SN where NM-MRI signal correlated negatively with DSC in the whole and limbic striatum. There were no significant associations between NM-MRI and DSC in the associative or sensorimotor striatum in HC and no significant associations in patients. These results show that NM-MRI signal and striatal DSC are negatively related in HC, but not in patients. Our results indicate that [$^{18}$F]F-DOPA PET and NM-MRI reflect different aspects of dopaminergic functioning. The negative correlation in HC might be explained by vesicular monoamine transporter-2 (VMAT-2) functioning. A lack of a correlation in patients might be due to the small sample size, effects of symptom severity or antipsychotic medication.

## 1. Introduction

[$^{18}$F]F-DOPA positron emission tomography (PET) is a well-established method for investigating striatal dopamine synthesis capacity (DSC). [$^{18}$F]F-DOPA PET studies have repeatedly demonstrated elevated striatal DSC (i.e. indicating striatal hyperdopaminergia), specifically in the associative striatum of patients with schizophrenia (Brugger et al., 2020; McCutcheon et al., 2018). PET imaging leads to (limited) radiation exposure to the patient and can be time-consuming and expensive. Therefore, new imaging methods have been developed to assess the dopaminergic system.

One promising tool that indirectly assesses dopaminergic functioning in the substantia nigra (SN) is neuromelanin-sensitive MRI (NM-MRI) (Cassidy et al., 2019). Neuromelanin is a black, insoluble pigment, that primarily accumulates in the dopaminergic neurons of the SN pars compacta (SNc) (Zecca et al., 2008). The deposition of neuromelanin depends on the amount of excess cytosolic dopamine that has not been transferred into synaptic vesicles (Sulzer et al., 2000; Zecca et al., 2008).

* Corresponding author. Maastricht University, P.O. Box 616, 6200 MD, Maastricht, the Netherlands.
*E-mail address:* carmen.vanhooijdonk@maastrichtuniversity.nl (C.F.M. van Hooijdonk).

https://doi.org/10.1016/j.nsa.2023.101134
Received 30 March 2023; Received in revised form 27 July 2023; Accepted 8 September 2023
Available online 14 September 2023

As a result of paramagnetic properties and magnetization transfer (MT) effects, neuromelanin-iron complexes cause T1-shortening (Trujillo et al., 2017). This creates a notable contrast in NM-MRI signal between the SN and the surrounding brain tissue. Multiple NM-MRI studies have demonstrated elevated neuromelanin concentration in the SN of patients with schizophrenia compared to healthy controls (HC) (Wieland et al., 2021).

The findings of elevated striatal DSC and neuromelanin concentration in the SN of patients with schizophrenia suggest that these measures might relate positively to each other. This is supported by the observation that NM-MRI signal in the SN is positively associated with amphetamine-induced dopamine release (i.e. another indicator of striatal hyperdopaminergia) in the whole striatum, as assessed with [$^{11}$C]raclopride PET, across patients with schizophrenia and HC (Cassidy et al., 2019). It is unknown though how striatal DSC and NM-MRI signal in the SN, as measures of nigrostriatal functioning, are interrelated. Therefore, we investigated the association between NM-MRI signal in the SN and DSC in the whole, associative, limbic, and sensorimotor striatum in HC and patients with a schizophrenia spectrum disorder (SSD). In addition, we explored the association between nigral DSC and NM-MRI signal in the SN of patients and HC. We hypothesized that NM-MRI signal in the SN is positively correlated with striatal DSC in both groups. We assessed the relation between NM-MRI signal and striatal DSC in separate groups since meta-analytic evidence shows that both measures are altered in patients with schizophrenia compared to controls (Brugger et al., 2020; McCutcheon et al., 2018; Wieland et al., 2021), and more importantly, striatal DSC seems to fluctuate with psychotic symptom severity and medication status in patients, (Gründer et al., 2003; Jauhar et al., 2017, 2018; Vernaleken et al., 2006), whereas there are indications that this is not the case for NM-MRI (unpublished data).

## 2. Material and methods

This study combines data from two patient and two HC cohorts, collected in the context of three Dutch studies approved by the Medical Ethical Committees of Leiden, The Hague, and Delft (NL72218.058.20), Amsterdam UMC, University of Amsterdam (NL63410.018.17), and the East Netherlands (NL72675.091.20). All participants gave written informed consent. PET data of all subjects have not been previously published. NM-MRI data of 9 patients are included in the analysis of another article (van der Pluijm et al., 2023).

### 2.1. Participants

For this study, early psychosis patients who recently experienced an episode of psychosis were recruited via two Dutch mental health institutes (details are explained in Methods S1). All patients were undergoing treatment and were diagnosed with SSD. Diagnoses were confirmed with the semi-structured Comprehensive Assessment of Symptoms and History (CASH) interview (Andreasen, 1987). In addition, HC matched for age, gender, smoking status, and educational level were recruited via social media. Patients and HC were both aged between 18 and 50 years. Exclusion criteria for patients included onset of first psychotic episode longer than five years ago and previous antipsychotic use longer than one year. Additional exclusion criteria are explained in Methods S1.

### 2.2. Design and procedures

Participants were assessed on 1 to 3 testing days. The study procedure consisted of: 1) screening for in- and exclusion criteria and completing measures on medication use (Methods S2) and symptom severity by use of the Positive and Negative Syndrome Scale (PANSS; patients only) (Kay et al., 1987) and the Beck Depression Inventory (BDI-II) (Beck et al., 1996; Van der Does, 2002); 2) MRI scan including the NM-MRI; and 3) [$^{18}$F]F-DOPA PET scan. Data collection occurred between March 11, 2019 and September 14, 2022.

### 2.3. NM-MRI acquisition

All participants were instructed to refrain from alcohol and cannabis 24 h before the MRI scan. MRI images were acquired on a 3T scanner (Phillips, Ingenia Elition X, Best, The Netherlands) with a 32-channel head coil at the Amsterdam UMC, the Netherlands. Structural whole-brain T1-weighted volumetric images were acquired for NM-MRI slice placement. NM-MRI was acquired with a T1-weighted 2D gradient echo sequence with MT pulse (TR = 260 ms; TE = 3.9 ms; 8 slices; FOV = 162 × 199 mm; in-plane resolution = 0.39 × 0.39 mm$^2$; slice thickness = 2.5 mm; number of signal averages = 2; FA = 40°; MT frequency offset = 1200 Hz; MT duration = 15.6 ms) (details of scan sequences are described in Methods S3).

### 2.4. NM-MRI pre-processing

The NM-MRI scans were pre-processed with a Matlab (MathWorks, Natrick, MA) pipeline (Wengler et al., 2020), which is extensively described in Methods S4. In short, NM-MRI images were coregistered to the T1-weighted images. Brain-extracted T1-weighted images were spatially normalized to Montreal Neurological Imaging (MNI) space. Next, the coregistered NM-MRI images were spatially normalized to MNI space using the warping parameters that were used for the normalization of the T1-weighted images. Afterwards, the normalized NM-MRI images were smoothed with a 1-mm full-width-at-half-maximum (FWHM) Gaussian kernel. The NM-MRI signal in the SN was calculated as a contrast-to-noise ratio (CNR) with the crus cerebri (CC) as the reference region, using SN and CC template masks (Fig. 1). For each participant, the CNR at each voxel v in the SN was calculated as the percent NM-MRI signal difference between a given voxel in the SN mask ($I_V$) and the mode of the signal intensity in the CC ($I_{CC}$) (Equation (1)). The mode of the signal intensity in the CC ($I_{CC}$) was calculated from a kernel distribution that was fitted to a histogram consisting of the NM-MRI signal values of all voxels within the CC mask.

$$\mathrm{CNR_V} = \left\{ \frac{[I_V - \mathrm{mode}(I_{CC})]}{\mathrm{mode}(I_{CC})} \right\} * 100 \qquad \text{(Equation 1)}$$

### 2.5. PET acquisition

All participants were asked to refrain from alcohol and cannabis 24 h, eating and drinking (except water) 6 h, and smoking 2 or 3 h before PET imaging. One hour before the PET scan, all participants received 150 mg carbidopa and 400 mg entacapone to block peripheral metabolization of [$^{18}$F]F-DOPA (Hoffman et al., 1992; Sawle et al., 1994). Before PET acquisition, a low-dose computed tomography (CT) scan of the brain was acquired for attenuation correction purposes. Subsequently, approximately 185 MBq [$^{18}$F]F-DOPA was administered as a single intravenous bolus injection. Immediately thereafter a 90-min dynamic PET acquisition started. PET data were acquired on a Siemens PET/CT system (Biograph mCT FlowTrue-V-128) (FOV = 256 × 256 mm; slice thickness = 2 mm; pixel spacing = 1.59 × 1.59 mm) and binned in 25 frames (5 × 1, 3 × 2, 3 × 3, and 14 × 5 min[s]) (Methods S5).

### 2.6. PET pre-processing

Details of the PET pre-processing are described in Methods S6. In short, participants who moved >7.5 mm during the data acquisition were excluded from further analyses, as attenuation correction might no longer be reliable. Structural T1-weighted and PET images were co-registered to a single PET frame acquired 7 min post-injection. Next, the T1-weighted images were segmented into white matter (WM), grey matter (GM), and cerebral spinal fluid (CSF). The volumes of interest (i.e. striatum and cerebellum) were generated based on Hammers' maximum

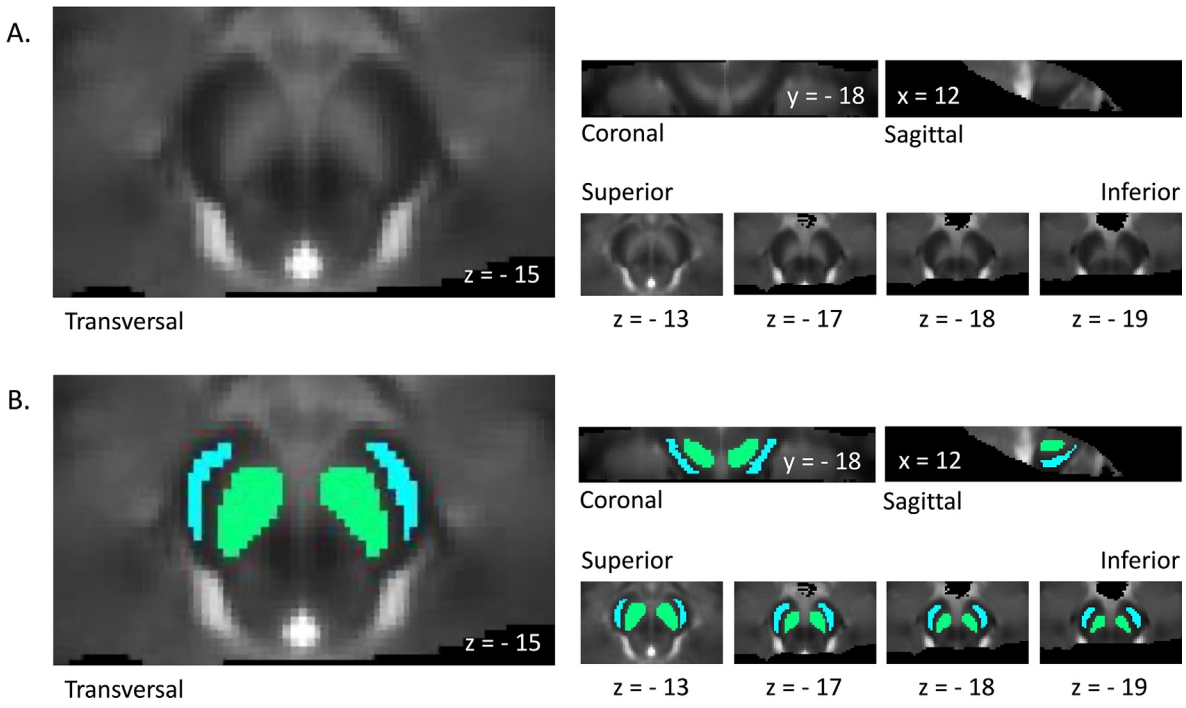


**Fig. 1.** Template masks of the substantia nigra and the crus cerebri
A. Average image of spatially normalized NM-MRI images from 28 participants included in the primary analyses. The SN is visible as a hyperintense area. B. Template masks of the SN (in green) and CC (in blue) in MNI space were created by manually tracing the regions on the average NM-MRI image. The template masks were used for calculating the contrast-to-noise ratio in all subjects. Abbreviations: CC, crus cerebri; MNI, Montreal Neurological Imaging; NM-MRI, neuromelanin-sensitive magnetic resonance imaging; SN, substantia nigra. (For interpretation of the references to colour in this figure legend, the reader is referred to the Web version of this article.)

probability atlas (Hammers et al., 2003). Afterwards, Patlak graphical analysis (Patlak and Blasberg, 1985) was used to calculate the influx constant $k_i^{cer}$ ($min^{-1}$; from here on labelled as $k_i^{cer}$) as a measure of DSC with the GM of the cerebellum as reference region. Linear fitting was conducted on the PET images acquired between 25 and 90 min to acquire a whole-brain parametric image (Fig. 2A/B). The $k_i^{cer}$ of the GM striatum was extracted from this parametric image.

A standard MNI brain template was warped with a non-linear affine transformation to the subject's MRI. Thereafter, the same transformation matrix was applied to warp the striatal subdivisions (i.e. associative, limbic, and sensorimotor striatum), as defined in the Oxford-GSK-Imanova brain atlas (Tziortzi et al., 2014), from MNI to subject space. Subsequently, the GM $k_i^{cer}$ for voxels with ≥90% probability of belonging to the striatal subdivision was extracted from the whole-brain parametric image. $k_i^{cer}$ in the SN was calculated with a similar method (Methods S6).

### 2.7. NM-MRI and PET analyses

In line with previous work, our primary analysis consisted of voxelwise analyses conducted in MATLAB (Cassidy et al., 2019, 2020). We chose voxelwise analyses to reduce statistical circularity in defining the SN region via signal-intensity thresholding and because the SN is a topographically heterogeneous region that comprises distinct tiers with differential projections and functional properties, for which there are no standard ROIs available yet. Age was used as a covariate in all analyses, as neuromelanin accumulation is known to be age-related (Xing et al., 2018). For the primary analysis, we examined the association between striatal DSC and nigral NM-MRI signal in both groups separately using a voxelwise robust linear regression with CNR as dependent variable and mean $k_i^{cer}$ values (for whole, associative, limbic, and sensorimotor striatum regions of interest [ROIs]) and age as independent variables (Methods S8). The voxelwise robust linear regression was performed for every voxel within the SN mask (i.e. 1480 voxels). To correct for multiple comparisons, significance testing was determined by use of a permutation test in which mean $k_i^{cer}$ values of the striatal ROI were randomly shuffled, 10,000 times, with respect to the individual maps of the NM-MRI signal in the SN. This resulted in a null distribution of the number of SN voxels that exceeded a threshold of $p < 0.050$. The permutation test corrects for multiple comparisons by deciding whether the effect's spatial extent (number of voxels showing an association with $ki^{cer}$) is larger compared to chance (corrected $p < 0.050$). In case of significant results, we subsequently performed post-hoc partial Spearman's rank-order correlation coefficient tests to address the strength of the correlation (i.e. Spearman's rho) between the mean $ki^{cer}$ of the striatal ROI and the mean CNR of the significant voxels as determined by the voxelwise analysis, with age as covariate. We calculated the 95%-confidence interval of Spearman's rho by use of the Fisher z-transformation. We performed the Spearman's tests with mean CNR values uncorrected and corrected for voxel selection (i.e. obtained by a leave-one-subject-out analysis to get an unbiased effect size). In the leave-one-out analysis, significant voxels for each HC were identified in a voxelwise analysis including the complete HC sample except the left-out subject. The significant voxels were used to extract the mean CNR for the left-out subject (i.e. corrected mean CNR). We explored the association between nigral DSC and NM-MRI signal in the SN with a similar voxel-based method. Group differences and associations between imaging and clinical variables were assessed as described in Methods S8.

## 3. Results

### 3.1. Sample characteristics

Eighteen patients with SSD and 24 HC completed the study. For various reasons, we were unable to use the data of 14 participants (n = 6 patients, n = 8 HC; Results S2). The final sample included 12 patients and 16 HC. Average head movement during the PET scan was comparable in

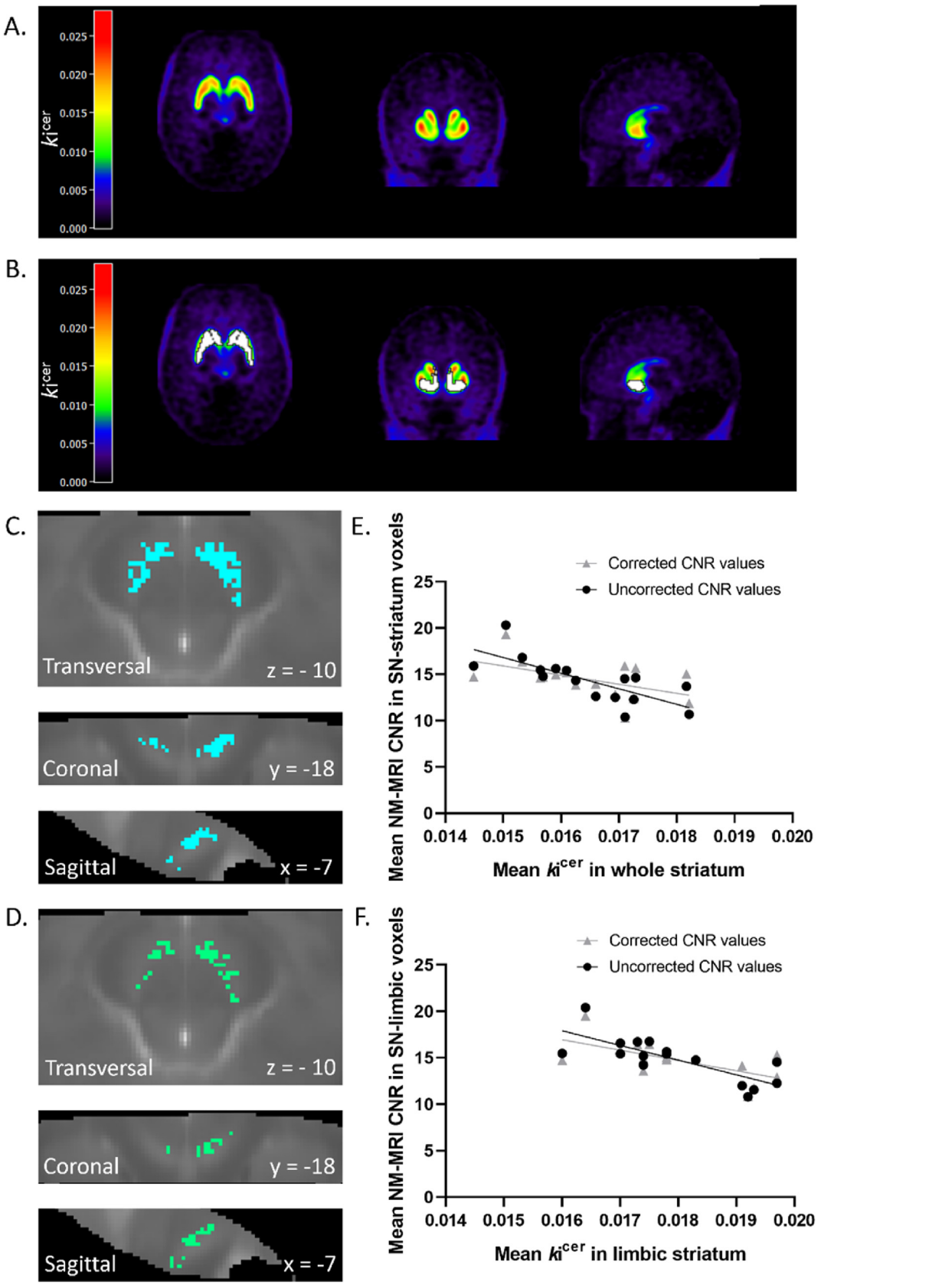


(caption on next page)

**Fig. 2.** Results of voxelwise analysis in the substantia nigra
(A) Average $k_i^{cer}$ in voxels throughout the brain of 16 healthy controls (HC) without and (B) with a mask of the limbic striatum (shown in white). The parametric image of each HC was converted to MNI space for visualization purposes. (C) Map of voxels (shown in blue) in which HC exhibit a negative correlation between NM-MRI contrast-to-noise ratio (CNR) and mean $k_i^{cer}$ values in the whole striatum (WS), i.e. SN-striatum voxels. (D) Map of voxels (shown in green) in which HC exhibit a negative correlation between CNR and mean $k_i^{cer}$ values in the limbic striatum (LST), i.e. SN-limbic voxels. (E) Scatterplot displaying the correlation between mean uncorrected and corrected for voxel selection CNR values in SN-striatum voxels and mean $k_i^{cer}$ value in the WS in HC (uncorrected: rho = −0.853, 95%-confidence interval (CI): (−0.560, −0.956), $p < 0.001$; corrected: rho = −0.445, 95%-CI: (−0.781, 0.091), $p = 0.097$). (F) Scatterplot displaying the correlation between mean uncorrected and corrected for voxel selection CNR values in SN-limbic voxels and mean $k_i^{cer}$ value in the LST in HC (uncorrected: rho = −0.840, 95%-CI: (−0.529, −0.952), $p < 0.001$; corrected: rho = −0.616, 95%-CI: (−0.125, −0.865), $p = 0.015$). (For interpretation of the references to colour in this figure legend, the reader is referred to the Web version of this article.)

these groups (patients: 2.39 mm, SD = 1.20; HC: 2.10 mm, SD = 1.20; Methods S9). There were no between-group differences in sex, age, current nicotine use, ethnicity, educational level, or injected [$^{18}$F]F-DOPA dose (Table 1). However, patients had significantly higher BDI scores compared to HC ($U = 6.000$, $p < 0.001$) and more lifetime cannabis use (i.e. ≤5 versus >5 times; $p = 0.047$). The voxelwise analysis to address group differences in CNR signal in the SN revealed no voxels with significant differences between groups (robust linear regression controlling for age, CNR patients > CNR HC corrected $p = 0.377$, CNR HC > CNR patients corrected $p = 0.760$, permutation test). We found no significant group differences for mean $k_i^{cer}$ values in the whole, associative, or limbic striatum, or the SN. Patients exhibited lower mean $k_i^{cer}$ values in the sensorimotor striatum than HC ($U = 45.000$; $p = 0.018$). This was no longer the case when using GM $k_i^{cer}$ of voxels with ≥60% instead of ≥90% probability of belonging to the sensorimotor striatum (Methods S7; Results S3). Non-specific uptake of [$^{18}$F]F-DOPA in the cerebellum was not significantly different in patients and HC (Fig. S1; Results S4).

### 3.2. Voxelwise and post-hoc analyses of the relationship between neuromelanin and DSC

We found a significant negative association in HC between mean $k_i^{cer}$ values in the whole striatum and CNR in a subset of voxels in the SN (hereafter called SN-striatum voxels; 218 of 1480 voxels at $p < 0.050$, robust linear regression controlling for age; corrected $p = 0.033$, permutation test; peak voxel MNI coordinates [x, y, z]: −5, −12, −9 mm; Fig. 2C). Similarly, we found a subset of voxels in the SN of HC (hereafter called SN-limbic voxels) that demonstrated a significant negative association between CNR and mean $k_i^{cer}$ values in the limbic striatum (333 of 1480 voxels at $p < 0.050$, robust linear regression controlling for age; corrected $p = 0.005$, permutation test; peak voxel MNI coordinates [x, y, z]: −6, −19, −13 mm; Fig. 2D). As previous research found a strong correlation between mean striatal $k_i^{cer}$ values for data from a 95-min and 60-min acquisition (Veronese et al., 2021), we performed a sensitivity analysis in which we repeated the voxelwise analysis for the whole and limbic striatum with four additional HC who were excluded due to movement. We applied linear fitting on the PET images of these four HC acquired between 25 min and the start of substantial (>7.5 mm) movement. Similarly to the previous findings, we found largely overlapping voxels within the SN where CNR significantly negatively correlated with $k_i^{cer}$ values in the whole and limbic striatum (whole striatum: $p = 0.021$; limbic striatum: $p = 0.015$; Results S5). We performed an additional sensitivity analysis in which we repeated the voxelwise analysis for the whole and limbic striatum without five HC who fasted for two instead of 6 h. This resulted in a borderline significant negative association between mean $k_i^{cer}$ values in the limbic striatum and CNR in a smaller (compared to the primary analysis) subset of voxels in the SN ($p = 0.051$; Results S6). The results for the whole striatum were no longer significant ($p = 0.167$).

There were no significant associations between CNR in the SN and mean $k_i^{cer}$ values in the associative and sensorimotor striatum in HC and no significant associations between CNR in the SN and mean $k_i^{cer}$ values in any of the striatal ROIs in patients (Results S7). We repeated the voxelwise analysis in patients for the whole and limbic striatum with three additional patients who were excluded due to movement. This resulted in non-significant findings (Results S5). The results of the striatal subdivisions did not change when using the mean $k_i^{cer}$ values with ≥60% instead of ≥90% probability of belonging to the striatal subdivision (Results S8). Our exploratory analyses revealed no subsets of voxels within the SN where CNR correlated significantly with mean $k_i^{cer}$ values in the SN in patients or HC (Results S9).

The post-hoc analyses revealed a significant negative correlation between the mean CNR in SN-striatum voxels and mean $k_i^{cer}$ values in the whole striatum of HC (controlling for age; uncorrected for voxel selection, rho = −0.853, 95%-CI: (−0.560, −0.956), $p < 0.001$; corrected for voxel selection, rho = −0.445, 95%-CI: (−0.781, 0.091), $p = 0.097$; Fig. 2E). In addition, we found a negative correlation between the mean CNR in SN-limbic voxels and mean $k_i^{cer}$ values in the limbic striatum of HC (controlling for age; uncorrected for voxel selection, rho = −0.840, 95%-CI: (−0.529, −0.952), $p < 0.001$; corrected for voxel selection, rho = −0.616, 95%-CI: (−0.125, −0.865), $p = 0.015$; Fig. 2F). For completeness, we also assessed the association between mean CNR within the whole SN mask and mean $k_i^{cer}$ values in the different ROIs with age as covariate (Results S10; Fig. S2). We found no significant associations. Exploratory findings of the relationships between imaging and clinical variables are described in Results S11-S14.

## 4. Discussion

We used NM-MRI and [$^{18}$F]F-DOPA PET imaging to investigate the association between NM-MRI signal in the SN and DSC in the striatum and SN of patients with SSD and HC. Contrary to our expectations, we found voxels within the SN of HC where NM-MRI signal correlated negatively with DSC in the whole and/or limbic striatum. The negative associations in the limbic subdivision of the striatum of HC were largely confirmed in post-hoc and sensitivity analyses and not found in patients. Our exploratory analysis did not reveal any significant association between DSC in the SN and NM-MRI signal, which is in line with earlier findings in HC (Ito et al., 2017).

Our finding of a negative correlation between NM-MRI and [$^{18}$F]F-DOPA measures in HC is surprising given that the accumulation of neuromelanin is mostly determined by the amount of excessive cytosolic dopamine (Sulzer et al., 2000). The negative correlation in HC might be explained by functioning of the vesicular monoamine transporter-2 (VMAT-2), which transports cytosolic dopamine into synaptic vesicles. VMAT-2 levels were found to be positively associated with tyrosine hydroxylase levels (i.e. the rate-limiting enzyme for dopamine synthesis, which synthesizes L-DOPA from tyrosine) and negatively associated with neuromelanin pigment in the ventral SN of post-mortem human brains (Liang et al., 2004). It might therefore be that dopaminergic neurons in the midbrain of HC with greater amounts of dopamine synthesis have more vesicular storage capacity and consequently less neuromelanin deposition in the SN. This is in line with the finding of Sulzer et al. (2000) who found that neuromelanin synthesis is inhibited by adenoviral-mediated overexpression of VMAT-2. In addition, in rat striata, VMAT-2 functionally and physically interacts with the enzymes tyrosine and aromatic acid decarboxylase (which synthesizes dopamine from L-DOPA) (Cartier et al., 2010), indicating that these components of the dopamine system are directly linked to each other. The negative association in HC suggests that NM-MRI and [$^{18}$F]F-DOPA PET reflect

**Table 1**
Sample characteristics.

| | Patients (n = 12) | Healthy controls (n = 16) | p-value |
|---|---|---|---|
| **Demographics and clinical characteristics** | | | |
| Sex (F/M) | 2/10 | 4/12 | 0.673[a] |
| Age in years, mean (SD) | 20.8 (2.7) | 24.5 (6.2) | 0.129[b] |
| Current nicotine use[c] (Yes/No) | 4/8 | 3/16 | 0.418[a] |
| Lifetime cannabis use (≤5 versus/>5 times) | 4/8 | 10/3[d] | **0.047**[a] |
| Education, No. | – | – | 0.125[a] |
| Secondary vocational education/ Senior general secondary education/ Pre-university education | 9 | 6 | – |
| Higher professional education/ University education (Bachelor's degree) | 3 | 9 | – |
| University education (Master's degree) | 0 | 1 | – |
| Ethnicity, No. (White/Other) | 10/2 | 15/1 | 0.560[a] |
| Injected [$^{18}$F]F-DOPA dose in MBq, mean (SD) | 180.6 (13.8) | 179.1 (15.5) | 0.963[b] |
| Number of days between [$^{18}$F]F-DOPA PET and NM-MRI, mean (range) | 14.8 (0–33) | 5.4 (0–71) | **0.001**[b] |
| PANSS at study enrollment | – | – | – |
| Positive score, mean (SD) | 12.2 (5.0) | NA | NA |
| Negative score, mean (SD) | 12.9 (6.2) | NA | NA |
| General score, mean (SD) | 25.1 (8.7) | NA | NA |
| Total score, mean (SD) | 50.2 (14.3) | NA | NA |
| BDI, mean (SD) | 12.8 (8.0) | 1.8 (2.1) | **<0.001**[b] |
| Current 100 mg CPZ-equivalent dose in mg, mean (SD)[e] | 398.6 (222.0) | NA | NA |
| Total days on antipsychotic medication, mean (SD)[e] | 122.1 (98.0) | NA | NA |
| CPZ dose-years, mean (SD)[e] | 0.078 (0.088) | NA | NA |
| Diagnosis, No. | – | – | – |
| Schizophrenia | 5 | NA | NA |
| Schizoaffective disorder | 2 | NA | NA |
| Schizophreniform disorder | 3 | NA | NA |
| Unspecified schizophrenia spectrum and other psychotic disorder | 1 | NA | NA |
| Other specified schizophrenia spectrum and other psychotic disorder | 1 | NA | NA |
| **NM-MRI and [$^{18}$F] F-DOPA PET outcome parameters** | | | |
| CNR, mean (SD)[f] | 15.3 (1.0) | 15.0 (1.6) | 0.889[b] |
| $ki^{cer}$ WS, mean (SD) | 0.0159 (0.0024) | 0.0164 (0.0011) | 0.227[b] |
| $ki^{cer}$ LST (0.9 threshold), mean (SD) | 0.0173 (0.0021) | 0.0179 (0.0012) | 0.163[b] |
| $ki^{cer}$ AST (0.9 threshold), mean (SD) | 0.0189 (0.0026) | 0.0194 (0.0014) | 0.486[b] |
| $ki^{cer}$ SMST (0.9 threshold), mean (SD) | 0.0196 (0.0037) | 0.0216 (0.0019) | **0.018**[b] |
| $ki^{cer}$ SN, mean (SD) | 0.0099 (0.0014) | 0.0099 (0.0011) | 0.329[b] |

Abbreviations: AST, associative striatum; BDI, Beck Depression Inventory; CNR, contrast-to-noise ratio; CPZ, chlorpromazine; F, female; LST, limbic striatum; M, male; MBq, megabecquerel; NA, not applicable; NM-MRI, neuromelanin-sensitive magnetic resonance imaging; PANSS, positive and negative symptom scale; PET, positron emission tomography; SD, standard deviation; SN, substantia nigra; SMST, sensorimotor striatum; WS, whole striatum. Significant results are bold.

[a] Group differences were assessed with Fisher's exact test.

[b] Group differences were assessed with the Mann-Whitney *U* test.

[c] Current nicotine use is defined as having used nicotine daily for at least one month in the past twelve months.

[d] Data on cannabis lifetime use of three healthy controls was missing, although they did not report any cannabis use in the six months before participation.

[e] During the first scan.

[f] Based on average for the whole SN mask (i.e. not the voxelwise analysis).

different components of the dopamine system. This is also supported by the fact that striatal [$^{18}$F]F-DOPA signal decreases with age (Kumakura et al., 2005), while NM-MRI signal increases with age (Xing et al., 2018).

We most consistently found a negative association between NM-MRI and [$^{18}$F]F-DOPA measures in HC for the limbic striatum. The significant findings in the whole striatum might therefore be driven by the association present in the limbic striatum. The voxels in the SN where NM-MRI signal correlated negatively with DSC in the limbic striatum (Fig. 2D) largely overlap with the medial SN, which is found to be connected to the ventral striatum (i.e. the anatomical subregion of the striatum previously classified as belonging to the limbic functional subdivision of the striatum) (Martinez et al., 2003; Zhang et al., 2017). In addition, the medial SN is anatomically adjacent to the ventral tegmental area (VTA) (Peterson et al., 2017), which innervates the nucleus accumbens and ventromedial striatum (i.e. mesolimbic dopaminergic pathway). The reason why the association with the limbic striatum is strongest is still unclear, although it is also known that VMAT-2 levels are lower in the more lateral parts of the ventral SN than in the medial parts of the SN (Liang et al., 2004).

The lack of a correlation in patients might be explained by the small sample size. Additionally, striatal DSC might fluctuate more over time in patients compared to HC, as striatal DSC is associated with psychotic symptom severity in patients (Jauhar et al., 2017, 2018). We did not find significant associations between symptom severity and striatal DSC in our sample, which might be due to the relatively low symptom severity in our patients. Illness severity, duration of illness, and antipsychotic medication might affect striatal DSC (Gründer et al., 2003; Vernaleken et al., 2006), whereas no changes in NM-MRI signal have been found after six months of antipsychotic treatment in patients with schizophrenia (unpublished data). This suggests that [$^{18}$F]F-DOPA PET might be a dynamic measure of DSC (i.e. state-like feature of schizophrenia), while as neuromelanin is a deposit, NM-MRI signal in the SN might reflect more chronic changes in dopamine synthesis (i.e. trait-like feature of schizophrenia). Moreover, in patients, the relationship between striatal DSC and VMAT-2 functioning might be dysfunctional. Although VMAT-2 function is unchanged in the striatum (Taylor et al., 2000) and VMAT-2 binding in the ventral brainstem has been found to be elevated in patients with schizophrenia compared to HC (Zubieta et al., 2001), a post-mortem study found decreased VMAT-2 mRNA levels in the SN of patients with schizophrenia (Purves-Tyson et al., 2017). This might indicate that in a subgroup of patients, increased DSC, which is suggested to be a core feature of the illness (Brugger et al., 2020), might not be accompanied by an increase in VMAT-2 functioning, which would consequently result in more cytosolic dopamine and thereby more deposition of neuromelanin. Finally, besides elevated striatal [$^{18}$F]F-DOPA utilization (i.e. the net blood-brain clearance), patients with schizophrenia also demonstrated reduced storage or retention of [$^{18}$F]-fluorodopamine within synaptic vesicles compared to HC (Kumakura et al., 2007). This would be in line with reduced VMAT-2 functioning in patients. Future studies should address [$^{18}$F]F-DOPA, VMAT-2, and NM-MRI measures in a large cohort of patients and HC to further elucidate the underlying relationships and their time-courses across the lifespan, while taking into account factors such as illness duration, symptom severity, antipsychotic medication, and seasonal effects (Eisenberg et al., 2010).

Previous studies reported elevated striatal DSC in patients with schizophrenia (Brugger et al., 2020). In contrast, we found a significantly lower mean DSC in the sensorimotor striatum and no differences in the other striatal ROIs in patients compared to HC. These inconsistencies might be due to remission of psychosis in some patients, as lower DSC has been reported in the whole, associative, and sensorimotor striatum of patients in psychotic remission (Avram et al., 2019; Brandl et al., 2022). The group difference in the sensorimotor striatum did not remain significant when using GM $k_i^{cer}$ of voxels with ≥60% instead of ≥90% probability of belonging to the sensorimotor striatum. This finding might therefore be an incidental finding. In addition, we found no significant

group differences for NM-MRI signal in the SN. This might be due to the small sample size or heterogeneity, as schizophrenia is a heterogeneous disorder and the existence of multiple subgroups of patients with varying neurobiology has been suggested (Howes and Kapur, 2014). Moreover, the conversion of dopamine to neuromelanin is promoted by iron. Previous research has demonstrated that the iron chelator desferrioxamine blocks the synthesis of neuromelanin (Sulzer et al., 2000) and others reported lower iron concentrations in subcortical brain regions of patients with SSD compared to controls (Sui et al., 2022; Xu et al., 2021). Consequently, changes in iron levels within the SN might also affect the formation of neuromelanin complexes.

A major strength of this study is that we are the first to combine NM-MRI and [$^{18}$F]F-DOPA PET in HC and patients with SSD. However, some limitations have to be taken into account. First, due to the difficulty in recruiting this study population, the sample size of our final sample is limited. To increase our sample size, we aggregated data from three studies with similar selection criteria that used the same NM-MRI and [$^{18}$F]F-DOPA PET protocols, except for the length of the fasting time. As [$^{18}$F]F-DOPA competes with other substrates for transport across the blood-brain barrier, this might have influenced the [$^{18}$F]F-DOPA PET results. The sensitivity analysis, without five HC that fasted for two instead of 6 h, remained borderline significant in the LST and was no longer significant for the whole striatum (Results S6), which is likely due to a lack of power. Second, [$^{18}$F]F-DOPA PET measures a combination of cellular processes (i.e. uptake and conversion of [$^{18}$F]F-DOPA, as well as, storage of [$^{18}$F]-fluorodopamine). Therefore, additional research needs to investigate which specific aspects of striatal DSC are associated with NM-MRI signal in the SN. This might be done with compartmental modelling in combination with arterial blood sampling during data collection, or by use of other PET tracers, such as 6-[$^{18}$F]Fluoro-l-*m*-tyrosine, which is not, unlike DOPA ligands, subject to transport into vesicles and post-release processes (Endres et al., 1997). Finally, some participants were regular smokers and/or recreationally used drugs (mainly cannabis). We included these subjects, as a substantial part of patients with SSD uses nicotine, alcohol, and cannabis, and excluding these subject will therefore make recruitment even more difficult and result in a non-representative sample. To limit the potential effect of cannabis use on our results, we did not include people who met criteria for a past or present cannabis use disorder. Participants that had used cannabis $<$6 times in a lifetime (n = 14) did not differ from participants that had used cannabis $\geq$6 times in a lifetime (n = 11; data of 3 HC was missing) with regard to mean $ki^{cer}$ values in the striatal ROIs or mean CNR in the SN. Moreover, we found no association between the number of cigarettes or cigars daily smoked by the tobacco users in our sample (4 patients; 2 HC; i.e. during the period when the subject used the most in the 12 months before study participation) and mean CNR in the SN or mean $ki^{cer}$ values in the whole, associative, limbic, and sensorimotor striatum or SN. Although acute effects of smoking on our imaging measures were likely to be small as the majority of subjects were nonsmokers and others were instructed to refrain from smoking 2 or 3 h before the [18F]F-DOPA PET scan, effects of smoking on striatal DSC are not yet completely understood and studies have reported higher (Salokangas et al., 2000), lower (Rademacher et al., 2016) and unchanged striatal DSC in smokers compared to nonsmokers (Bloomfield et al., 2014a). Further studies are needed to examine the short- and long-term effects of smoking on striatal DSC. Katthagen et al. (2020) demonstrated that patients with schizophrenia and without comorbid alcohol abuse (n = 10) have increased DSC in the left sensorimotor striatum compared to patients with schizophrenia and alcohol abuse (ICD-10 criteria; n = 7). To constrain the short-term effect of alcohol use on the imaging measures, all participants were instructed to refrain from alcohol 24 h before the MRI and PET scans. Moreover, none of the subjects reported drinking behaviour that would meet ICD-10 criteria for alcohol abuse and, therefore, lower sDSC in the sensorimotor striatum of patients seems unrelated to the drinking behaviour of these patients. Finally, we expect that previous recreational drug use had little effect on our outcome measures, as we selected participants with little to no drug use, who were not dependent on any substance (Bloomfield et al., 2014b).

## 5. Conclusions

NM-MRI and [$^{18}$F]F-DOPA PET are negatively related to each other in HC, but not significantly in patients with SSD. These results indicate that [$^{18}$F]F-DOPA PET and NM-MRI are measures that reflect different aspects of dopaminergic functioning. We hypothesize that the negative correlation between neuromelanin and striatal DSC in HC might be explained by VMAT-2 functioning. A lack of a correlation in patients might be due to the small sample size or might be explained by effects of symptom severity or antipsychotic medication. In addition, striatal [$^{18}$F]F-DOPA PET might reflect a dynamic, state-like, aspect of dopaminergic functioning, while NM-MRI signal in the SN might reflect a chronic, trait-like, aspect of dopaminergic functioning. Future studies should assess the interrelationships between DSC, neuromelanin, VMAT-2, and related processes in larger homogeneous cohorts. As NM-MRI is more accessible than PET imaging, this might eventually enable clinicians and researchers to study specific aspects of the dopaminergic system of humans more efficiently and at lower costs.

## Author contributions

CvH, MvdP, MH, RvH, LdH, JPS, TvA, JB, and EvdG designed and planned the study. CvH, MvdP, and MH performed the data collection. CvH, CS, and MvdP analyzed the data under the supervision of EvdG, FvV, GH, KW, and MY. CvH wrote the original draft of the manuscript. All authors reviewed and edited the manuscript. All authors have read and agreed to the published version of the manuscript.

## Funding

This work was supported in part by a Veni grant (91618075) from the Netherlands Organisation for Health Research and Development (ZonMw) (EvdG), Stichting J.M.C. Kapteinfonds (JPS), and NWO/Aspasia grant (RvH). The funders had no role in the study design, data collection or analysis, decision to publish, or preparation of the manuscript.

## Declaration of competing interest

All authors declare that they have no conflict of interest.

## Acknowledgements

We would like to thank all subjects for participating in this study.

## Appendix A. Supplementary data

Supplementary data to this article can be found online at https://doi.org/10.1016/j.nsa.2023.101134.

## References

Andreasen, N.C., 1987. Comprehensive Assessment of Symptoms and History (CASH). Department of Psychiatry, University of Iowa College of Medicine.

Avram, M., Brandl, F., Cabello, J., Leucht, C., Scherr, M., Mustafa, M., Leucht, S., Ziegler, S., Sorg, C., 2019. Reduced striatal dopamine synthesis capacity in patients with schizophrenia during remission of positive symptoms. Brain 142, 1813–1826.

Beck, A.T., Steer, R.A., Brown, G.K., 1996. Manual for the Beck Depression Inventory-II, vol. 1. Psychological Corporation, San Antonio, TX, pp. 10–1037.

Bloomfield, M.A., Pepper, F., Egerton, A., Demjaha, A., Tomasi, G., Mouchlianitis, E., Maximen, L., Veronese, M., Turkheimer, F., Selvaraj, S., 2014a. Dopamine function in cigarette smokers: an [18F]-DOPA PET study. Neuropsychopharmacology 39, 2397–2404.

Bloomfield, M.A., Morgan, C.J., Egerton, A., Kapur, S., Curran, H.V., Howes, O.D., 2014b. Dopaminergic function in cannabis users and its relationship to cannabis-induced psychotic symptoms. Biol. Psychiatr. 75, 470–478.

Brandl, F., Knolle, F., Avram, M., Leucht, C., Yakushev, I., Priller, J., Leucht, S., Ziegler, S., Wunderlich, K., Sorg, C., 2022. Negative symptoms, striatal dopamine and model-free reward decision-making in schizophrenia. Brain.

Brugger, S.P., Angelescu, I., Abi-Dargham, A., Mizrahi, R., Shahrezaei, V., Howes, O.D., 2020. Heterogeneity of striatal dopamine function in schizophrenia: meta-analysis of variance. Biol. Psychiatr. 87, 215–224.

Cartier, E.A., Parra, L.A., Baust, T.B., Quiroz, M., Salazar, G., Faundez, V., Egana, L., Torres, G.E., 2010. A biochemical and functional protein complex involving dopamine synthesis and transport into synaptic vesicles. J. Biol. Chem. 285, 1957–1966.

Cassidy, C.M., Carpenter, K.M., Konova, A.B., Cheung, V., Grassetti, A., Zecca, L., Abi-Dargham, A., Martinez, D., Horga, G., 2020. Evidence for dopamine abnormalities in the substantia nigra in cocaine addiction revealed by neuromelanin-sensitive MRI. Am. J. Psychiatr. 177, 1038–1047.

Cassidy, C.M., Zucca, F.A., Girgis, R.R., Baker, S.C., Weinstein, J.J., Sharp, M.E., Bellei, C., Valmadre, A., Vanegas, N., Kegeles, L.S., 2019. Neuromelanin-sensitive MRI as a noninvasive proxy measure of dopamine function in the human brain. Proc. Natl. Acad. Sci. USA 116, 5108–5117.

Eisenberg, D.P., Kohn, P.D., Baller, E.B., Bronstein, J.A., Masdeu, J.C., Berman, K.F., 2010. Seasonal effects on human striatal presynaptic dopamine synthesis. J. Neurosci. 30, 14691–14694.

Endres, C.J., Swaminathan, S., DeJesus, O.T., Sievert, M., Ruoho, A.E., Murali, D., Rommelfanger, S.G., Holden, J.E., 1997. Affinities of dopamine analogs for monoamine granular and plasma membrane transporters: implications for PET dopamine studies. Life Sci. 60, 2399–2406.

Gründer, G., Vernaleken, I., Müller, M.J., Davids, E., Heydari, N., Buchholz, H.G., Bartenstein, P., Munk, O.L., Stoeter, P., Wong, D.F., 2003. Subchronic haloperidol downregulates dopamine synthesis capacity in the brain of schizophrenic patients in vivo. Neuropsychopharmacology 28, 787–794.

Hammers, A., Allom, R., Koepp, M.J., Free, S.L., Myers, R., Lemieux, L., Mitchell, T.N., Brooks, D.J., Duncan, J.S., 2003. Three-dimensional maximum probability atlas of the human brain, with particular reference to the temporal lobe. Hum. Brain Mapp. 19, 224–247.

Hoffman, J.M., Melega, W.P., Hawk, T.C., Grafton, S.C., Luxen, A., Mahoney, D.K., Barrio, J.R., Huang, S.C., Mazziotta, J.C., Phelps, M.E., 1992. The effects of carbidopa administration on 6-[18F] fluoro-L-dopa kinetics in positron emission tomography. J. Nucl. Med. 33, 1472–1477.

Howes, O.D., Kapur, S., 2014. A neurobiological hypothesis for the classification of schizophrenia: type A (hyperdopaminergic) and type B (normodopaminergic). Br. J. Psychiatr. 205, 1–3.

Ito, H., Kawaguchi, H., Kodaka, F., Takuwa, H., Ikoma, Y., Shimada, H., Kimura, Y., Seki, C., Kubo, H., Ishii, S., 2017. Normative data of dopaminergic neurotransmission functions in substantia nigra measured with MRI and PET: neuromelanin, dopamine synthesis, dopamine transporters, and dopamine D2 receptors. Neuroimage 158, 12–17.

Jauhar, S., McCutcheon, R., Borgan, F., Veronese, M., Nour, M., Pepper, F., Rogdaki, M., Stone, J., Egerton, A., Turkheimer, F., 2018. The relationship between cortical glutamate and striatal dopamine in first-episode psychosis: a cross-sectional multimodal PET and magnetic resonance spectroscopy imaging study. Lancet Psychiatr. 5, 816–823.

Jauhar, S., Nour, M.M., Veronese, M., Rogdaki, M., Bonoldi, I., Azis, M., Turkheimer, F., McGuire, P., Young, A.H., Howes, O.D., 2017. A test of the transdiagnostic dopamine hypothesis of psychosis using positron emission tomographic imaging in bipolar affective disorder and schizophrenia. JAMA Psychiatr. 74, 1206–1213.

Kay, S.R., Fiszbein, A., Opler, L.A., 1987. The positive and negative syndrome scale (PANSS) for schizophrenia. Schizophr. Bull. 13, 261–276.

Katthagen, T., Kaminski, J., Heinz, A., Buchert, R., Schlagenhauf, F., 2020. Striatal dopamine and reward prediction error signaling in unmedicated schizophrenia patients. Schizophr. Bull. 46 (6), 1535–1546.

Kumakura, Y., Cumming, P., Vernaleken, I., Buchholz, H.G., Siessmeier, T., Heinz, A., Kienast, T., Bartenstein, P., Gründer, G., 2007. Elevated [18F] fluorodopamine turnover in brain of patients with schizophrenia: an [18F] fluorodopa/positron emission tomography study. J. Neurosci. 27, 8080–8087.

Kumakura, Y., Vernaleken, I., Gründer, G., Bartenstein, P., Gjedde, A., Cumming, P., 2005. PET studies of net Blood—brain clearance of FDOPA to human brain: age-dependent decline of [18F] Fluorodopamine storage capacity. J. Cerebr. Blood Flow Metabol. 25, 807–819.

Liang, C.L., Nelson, O., Yazdani, U., Pasbakhsh, P., German, D.C., 2004. Inverse relationship between the contents of neuromelanin pigment and the vesicular monoamine transporter-2: human midbrain dopamine neurons. J. Comp. Neurol. 473, 97–106.

Martinez, D., Slifstein, M., Broft, A., Mawlawi, O., Hwang, D.R., Huang, Y., Cooper, T., Kegeles, L., Zarahn, E., Abi-Dargham, A., 2003. Imaging human mesolimbic dopamine transmission with positron emission tomography. Part II: amphetamine-induced dopamine release in the functional subdivisions of the striatum. J. Cerebr. Blood Flow Metabol. 23, 285–300.

McCutcheon, R., Beck, K., Jauhar, S., Howes, O.D., 2018. Defining the locus of dopaminergic dysfunction in schizophrenia: a meta-analysis and test of the mesolimbic hypothesis. Schizophr. Bull. 44, 1301–1311.

Patlak, C.S., Blasberg, R.G., 1985. Graphical evaluation of blood-to-brain transfer constants from multiple-time uptake data. Generalizations. J. Cerebr. Blood Flow Metabol. 5, 584–590.

Peterson, A.C., Zhang, S., Hu, S., Chao, H.H., Li, C.S.R., 2017. The effects of age, from young to middle adulthood, and gender on resting state functional connectivity of the dopaminergic midbrain. Front. Hum. Neurosci. 11, 52.

Purves-Tyson, T., Owens, S., Rothmond, D., Halliday, G., Double, K., Stevens, J., McCrossin, T., Shannon Weickert, C., 2017. Putative presynaptic dopamine dysregulation in schizophrenia is supported by molecular evidence from post-mortem human midbrain. Transl. Psychiatry 7 e1003-e1003.

Rademacher, L., Prinz, S., Winz, O., Henkel, K., Dietrich, C.A., Schmaljohann, J., Shali, S.M., Schabram, I., Stoppe, C., Cumming, P., 2016. Effects of smoking cessation on presynaptic dopamine function of addicted male smokers. Biol. Psychiatr. 80, 198–206.

Salokangas, R.K., Vilkman, H., Ilonen, T., Taiminen, T., Bergman, J.n., Haaparanta, M., Solin, O., Alanen, A., Syvälahti, E., Hietala, J., 2000. High levels of dopamine activity in the basal ganglia of cigarette smokers. Am. J. Psychiatr. 157, 632–634.

Sawle, G., Burn, D., Morrish, P., Lammertsma, A., Snow, B., Luthra, S., Osman, S., Brooks, D., 1994. The effect of entacapone (OR-611) on brain [18F]-6-L-fluorodopa metabolism: implications for levodopa therapy of Parkinson's disease. Neurology 44, 1292-1292.

Sui, Y.V., McKenna, F., Bertisch, H., Storey, P., Anthopolos, R., Goff, D.C., Samsonov, A., Lazar, M., 2022. Decreased basal ganglia and thalamic iron in early psychotic spectrum disorders are associated with increased psychotic and schizotypal symptoms. Mol. Psychiatr. 27 (12), 5144–5153.

Sulzer, D., Bogulavsky, J., Larsen, K.E., Behr, G., Karatekin, E., Kleinman, M.H., Turro, N., Krantz, D., Edwards, R.H., Greene, L.A., 2000. Neuromelanin biosynthesis is driven by excess cytosolic catecholamines not accumulated by synaptic vesicles. Proc. Natl. Acad. Sci. USA 97, 11869–11874.

Taylor, S.F., Koeppe, R.A., Tandon, R., Zubieta, J.K., Frey, K.A., 2000. In vivo measurement of the vesicular monoamine transporter in schizophrenia. Neuropsychopharmacology 23, 667–675.

Trujillo, P., Summers, P.E., Ferrari, E., Zucca, F.A., Sturini, M., Mainardi, L.T., Cerutti, S., Smith, A.K., Smith, S.A., Zecca, L., 2017. Contrast mechanisms associated with neuromelanin-MRI. Magn. Reson. Med. 78, 1790–1800.

Tziortzi, A.C., Haber, S.N., Searle, G.E., Tsoumpas, C., Long, C.J., Shotbolt, P., Douaud, G., Jbabdi, S., Behrens, T.E., Rabiner, E.A., 2014. Connectivity-based functional analysis of dopamine release in the striatum using diffusion-weighted MRI and positron emission tomography. Cerebr. Cortex 24, 1165–1177.

Van Der Does, A., 2002. De Nederlandse versie van de Beck depression inventory, tweede editie. [The Dutch version of the Beck depression inventory. In: Lisse, The Netherlands: Swets & Zeitlinger, second ed.

van der Pluijm, M., Wengler, K., Reijers, P.N., Cassidy, C., Joe, K.T.T.T., de Peuter, O.R., Horga, G., Booij, L., de Haan, L., van de Giessen, E.M., 2023. Neuromelanin-sensitive MRI as candidate marker for treatment resistance in first episode schizophrenia. Am. J. Psychiatr. AJP 20220780.

Vernaleken, I., Kumakura, Y., Cumming, P., Buchholz, H.G., Siessmeier, T., Stoeter, P., Müller, M.J., Bartenstein, P., Gründer, G., 2006. Modulation of [18F] fluorodopa (FDOPA) kinetics in the brain of healthy volunteers after acute haloperidol challenge. Neuroimage 30, 1332–1339.

Veronese, M., Santangelo, B., Jauhar, S., D'Ambrosio, E., Demjaha, A., Salimbeni, H., Huajie, J., McCrone, P., Turkheimer, F., Howes, O., 2021. A potential biomarker for treatment stratification in psychosis: evaluation of an [18F] FDOPA PET imaging approach. Neuropsychopharmacology 46, 1122–1132.

Wengler, K., He, X., Abi-Dargham, A., Horga, G., 2020. Reproducibility assessment of neuromelanin-sensitive magnetic resonance imaging protocols for region-of-interest and voxelwise analyses. Neuroimage 208, 116457.

Wieland, L., Fromm, S., Hetzer, S., Schlagenhauf, F., Kaminski, J., 2021. Neuromelanin-sensitive magnetic resonance imaging in schizophrenia: a meta-analysis of case-control studies. Front. Psychiatr. 12.

Xing, Y., Sapuan, A., Dineen, R.A., Auer, D.P., 2018. Life span pigmentation changes of the substantia nigra detected by neuromelanin-sensitive MRI. Mov. Disord. 33, 1792–1799.

Xu, M., Guo, Y., Cheng, J., Xue, K., Yang, M., Song, X., Feng, Y., Cheng, J., 2021. Brain iron assessment in patients with First-episode schizophrenia using quantitative susceptibility mapping. Neuroimage Clinic 31, 102736.

Zecca, L., Bellei, C., Costi, P., Albertini, A., Monzani, E., Casella, L., Gallorini, M., Bergamaschi, L., Moscatelli, A., Turro, N.J., 2008. New melanic pigments in the human brain that accumulate in aging and block environmental toxic metals. Proc. Natl. Acad. Sci. USA 105, 17567–17572.

Zhang, Y., Larcher, K.M.H., Misic, B., Dagher, A., 2017. Anatomical and functional organization of the human substantia nigra and its connections. Elife 6, e26653.

Zubieta, J.K., Taylor, S.F., Huguelet, P., Koeppe, R.A., Kilbourn, M.R., Frey, K.A., 2001. Vesicular monoamine transporter concentrations in bipolar disorder type I, schizophrenia, and healthy subjects. Biol. Psychiatr. 49, 110–116.